Journal of Alloys and Compounds 499 (2010) 176–182

Contents lists available at ScienceDirect

Journal of Alloys and Compounds

journal homepage: www.elsevier.com/locate/jallcom

A new type of ⟨0 0 1⟩ junction observed in a (B2) Fe–Al–Ni–B alloy by TEM *in situ* straining

Anna Fraczkiewicz[a,*], Brigitte Decamps[b], David Colas[a], Olivier Calonne[a,1], François Louchet[c]

[a] PECM, UMR CNRS 5146, Ecole des Mines de St-Etienne, Centre SMS, 158 Cours Fauriel, 42100 St-Etienne, France
[b] CSNSM, UMR CNRS 8609, Université Paris-Sud, 91405 Orsay, France
[c] LGGE, UMR 5183 CNRS, Domaine Universitaire BP96, 38402 St Martin d'Heres, France

ARTICLE INFO

Article history:
Received 7 August 2009
Received in revised form 3 March 2010
Accepted 4 March 2010
Available online 11 March 2010

Keywords:
Intermetallics
Mechanical properties
Dislocations
TEM
FeAl

ABSTRACT

Single crystal foils of an FeAl alloy containing Ni and B are strained at elevated temperatures in an *in situ* dedicated transmission electron microscope (TEM). The observed characteristic "fork-shaped" dislocation configurations are shown to be a kind of "⟨0 0 1⟩ junction". This junction comes from a reaction between two ⟨1 1 1⟩ superdislocations gliding on different {1 1 2} planes; it results in the presence of a long and sessile edge ⟨0 0 1⟩ dislocation along the intersection of the glide planes. Several hypothetical core structures of such a junction are proposed and their possible effects on macroscopic mechanical properties of the alloy are discussed.

1. Introduction

In spite of numerous studies, the main characteristics of B2-ordered FeAl alloys are still not fully understood. The specific phenomenon of yield strength anomaly (YSA) [1–4] observed in these alloys is surely related to their unique ability to form (and to retain) high concentrations of thermal vacancies, but is also associated with complex dislocation processes [5–9,13]. A significant number of papers has been devoted to the study of dislocations in FeAl, especially using oriented single crystals [9–12,14] as well as specific deformation modes (*in situ* TEM testing [14]).

Dislocation processes in FeAl involve different types of defects. The shortest Burgers vector in a disordered body-centred cubic (bcc) lattice is $a/2\langle 1\,1\,1\rangle$. In the ordered B2 structure, these dislocations exist as superdislocations, consisting of pairs of $a/2\langle 1\,1\,1\rangle$ superpartials, separated by an antiphase boundary (APB). Their line energy is therefore larger than that of so-called ordinary dislocations, with $a\langle 1\,0\,0\rangle$ Burgers vectors, that are also observed.

In various B2 lattices, $a\langle 1\,0\,0\rangle$ ordinary or $a\langle 1\,1\,1\rangle$ superdislocations may dominate, depending on the APB energy (E_{APB}) [15]: for high E_{APB} values (e.g. NiAl), ordinary $a\langle 1\,0\,0\rangle$ dislocations are stable at room temperature, while lower E_{APB} values favour $a\langle 1\,1\,1\rangle$ superdislocations. FeAl alloys belong to the latter case: $a\langle 1\,1\,1\rangle$ superdislocations are commonly agreed to ensure plastic deformation at least at low temperatures [5,11,16], i.e. typically below 400–450 °C (depending on aluminium content). As in the disordered bcc lattice, different slip planes for ⟨1 1 1⟩ dislocations are possible: superdislocations are shown to glide mainly on {1 1 0} planes, but {1 1 2} and {1 2 3} glide planes have also been observed [11,16,17]. It seems also that the frequency of {1 1 2} glide increases with temperature [5].

The slip direction in FeAl above the YSA peak temperature remains a subject of debate. Some authors consider that only ⟨1 1 1⟩ dislocations are active in these materials at all the temperature ranges [1,4]. Yet, several experimental observations [9] suggest that ordinary $a\langle 1\,0\,0\rangle$ dislocations become active above the YSA peak. In fact, in the YSA domain of temperatures, between 400 and 700 °C (with exact temperature values that strongly depend on alloy composition and straining conditions), not only both $a\langle 1\,1\,1\rangle$ and $a\langle 1\,0\,0\rangle$ dislocations are observed, but $a\langle 1\,1\,0\rangle$ dislocations are also present. This latter Burgers vector may result from the superdislocation decomposition reaction [5,6,18]:

$$a\langle 1\,1\,1\rangle = a\langle 1\,1\,0\rangle + a\langle 0\,0\,1\rangle$$

There is circumstantial evidence that this kind of decomposition process may be at the origin of ordinary $a\langle 1\,0\,0\rangle$ dislocations observed at high temperatures. Yet, their role in the YSA phenomenon was not clear until now.

* Corresponding author. Tel.: +33 4 77 42 00 68; fax: +33 4 77 42 01 57.
E-mail address: anna.fraczkiewicz@emse.fr (A. Fraczkiewicz).
[1] Now at: AREVA Technical Center, 71205 Le Creusot, France.

0925-8388/$ – see front matter © 2010 Elsevier B.V. All rights reserved.
doi:10.1016/j.jallcom.2010.03.058

Table 1
Chemical composition of the studied alloy.

Alloy	Al (at.%)		Ni (at.%)		B (at.%)	
	Nominal	Analysed	Nominal	Analysed	Nominal	Analysed
FeAlNi4B	40	40.2	3.8	3.8	0.04	0.041

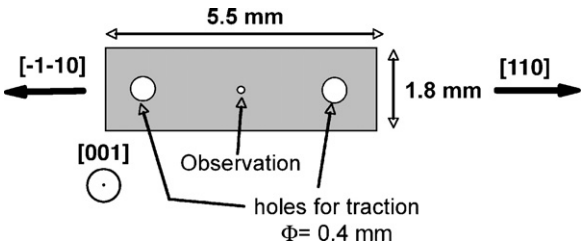

Fig. 1. Scheme of the thin foil used for *in situ* straining TEM experiments.

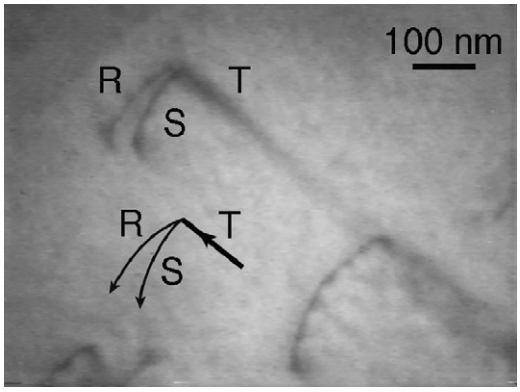

Fig. 2. A "fork-shaped" configuration. Extracted from [23]. FeAl4NiB single crystal, *in situ* deformed in a TEM at 600 °C. Bright field image, **g** = 1 1 0. A scheme of the configuration indicating the chosen orientation of the dislocation lines for the description of the Burgers vectors is given in inset. The tensile force is applied in the [1 1 0] direction.

The present work deals with intermediate temperature deformation of FeAl containing Ni and B. Samples were deformed at 600 °C, i.e. near the yield stress (YS) peak temperature, by *in situ* straining experiments in a specially equipped transmission electron microscope (TEM). Characteristic "fork-shaped" dislocation configurations are observed. Their crystallographic analysis is performed and possible influence on the material behaviour is discussed.

2. Materials and methods

A single crystal of an FeAlNiB alloy was grown by the horizontal Bridgman method from a high purity alloy prepared in the *Ecole des Mines* laboratory by a cold-crucible method. The chemical composition of the studied single crystal is given in Table 1.

Before testing, samples were annealed at 500 °C during 1 week to ensure an equilibrium concentration of vacancies [19]. Thin foils for *in situ* straining TEM experiments were cut from the grown single crystal using a precision "no stress-inducing" wire saw into rectangular foils (5.5 mm × 1.8 mm) about 100 μm thick. The foil plane is parallel to (0 0 1) and the straining direction is along [1 1 0] (Fig. 1). Finally, the central areas of the slices were thinned using a standard TEM electropolishing method [19] in a TENUPOL 5 (Struers) device.

In situ straining experiments were carried out using a custom JEOL 3010 TEM (LTPCM/SIMAP, Grenoble). This microscope operates at 300 kV and is equipped with a heating–straining double tilt stage, which provides a maximum load of 15 N between room temperature and 800 °C. Its tilting amplitude (of ±30° in "α" direction and +13°/−8° in the "β" one) helps to reach two-beam conditions convenient for defect analysis.

Samples were first slowly heated up to 600 °C under minimal stress, just enough to hold the foil clamped in the stage jaws. Mechanical testing started once the test temperature was reached; the estimated straining rate was about 10^{-4} s^{-1} [20]. Dynamic images were recorded using a digital video camera. When needed, the thin foil was slightly tilted to reach two-beam observation conditions. A static diffraction pattern was recorded at the beginning of each dynamic experiment to verify the sample orientation.

Postmortem analyses of *in situ* deformed foils were used to analyse dislocations. Burgers vectors, defined using the FS/RH convention [21], are determined through the classic extinction criterion ($|\vec{\mathbf{g}} \cdot \vec{\mathbf{b}}| = \mathbf{0}$) [22]. Dislocation line directions and corresponding slip planes are determined using a standard projection analysis.

3. *In situ* TEM observations

In our testing conditions, the alloy microstructure reveals a large number of specific "fork-shaped" dislocation configurations (Fig. 2), composed of two short segments (**R** and **S**) connected to the straight and heavily contrasted one (**T**). The complete video sequence of the experiment can be found *on-line* in Ref. [23]. *In situ* observations show that **R** and **S** segments move under stress, but that their junction dislocation **T** does not. Still, at least in the first stages of the progress of the "fork-shaped" configuration, the length of the **T** segment increases, due to the motion of **R** and **S** segments.

The further movement of fork-shaped configurations consists of an expansion of individual loops originating from **R** or **S** segments. In the sequence shown in Fig. 3, the **S** segment first begins to overtake the **R**-one (t = 43 s). At t = 63 s and t = 81 s, the **R** segment seems to be locked while the **S** starts developing a loop. The loop development takes place from t = 81 s to t = 182 s involving a reaction of the **S** segment with the original **T** segment (from t = 94 s to t = 119 s), leading to a local "unzipping" of the **T** segment. Due to the large expansion of the loop, its interaction with the foil surface is observed at t = 182 s, where a part of the loop disappears at the surface. It is worth noting that in the following stages of dislocation motion in Fig. 3, another loop, similar to that shown previously (t = 165 and 182 s), is observed a few seconds later (t = 223 s). It seems likely that this new loop has been developed from the now moving **R** segment. Let us also note that the parallel lines (marked "**W**", t = 150 s) come from other dislocation reactions, which are not involved in the present study.

Before starting a quantitative analysis of the dislocations involved in fork-shaped configurations, a few preliminary statements can already be made from the above observations.

(i) The projection of **T** on the observation plane is contained in the (1 1 0) plane.
(ii) The extension of **T** due to the motion of **R** and **S** segments has sometimes been observed to occur on distances as long as several micrometers, without any significant contrast modification. This suggests that the **T** segment is contained in the (0 0 1) foil plane. Since the foil plane is almost perpendicular to the electron beam in Fig. 3, the **T** segment coincides with its projection and is therefore parallel to the [−1 1 0] direction.
(iii) The **R** and **S** segments have been shown to be able to exchange their relative positions: if at the beginning of a sequence (Fig. 3), **R** seems to precede the **S** segment, it happens that the latter overtakes the former. Obviously, such an observation may only result from a 3D configuration projected along the electron beam direction. The **R** and **S** segments glide on non-parallel planes intersecting along [−1 1 0]: the **T** segment, formed by a reaction between **R** and **S**, is located along the common [−1 1 0] direction of **R** and **S** glide planes. The oscillating contrast of **S** and **R** segments indicates that they are situated in planes that are inclined with respect to the foil surface, in contrast with the **T** segment. It is also worth noting that such a configuration excludes dislocation glide on {1 1 0} planes.
(iv) Finally, loops that develop from **S** (or **R**) initial segments show a highly anisotropic shape (see Fig. 3, t = 165 s), with

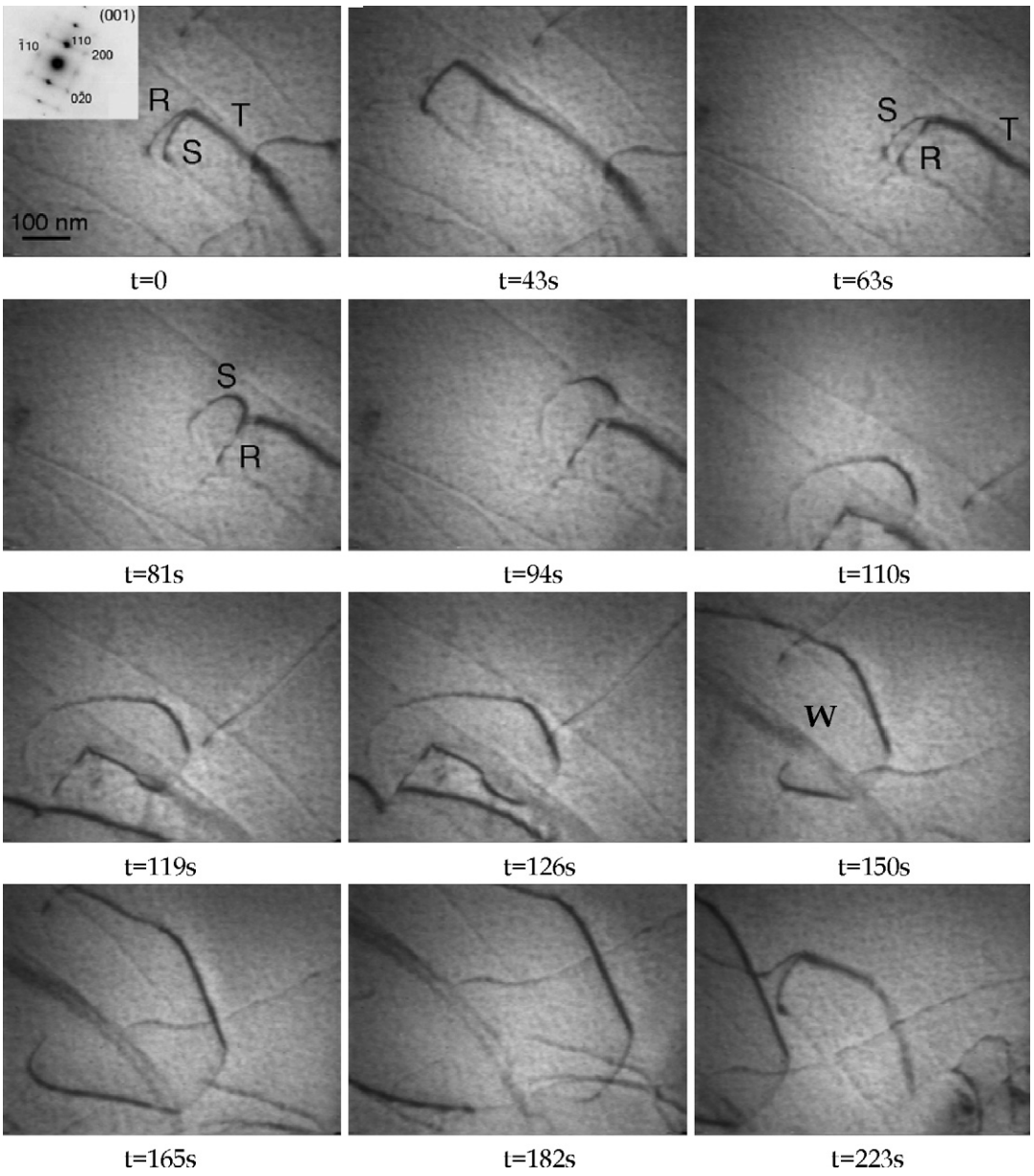

Fig. 3. Micrographs extracted from a video sequence [23] showing the formation and the evolution of a glissile loop from the **S** segment. The marker **W** indicates parallel lines that come from dislocations not involved in the analysed configuration. The tensile force is applied in the [1 1 0] direction.

straight-lined segments and local contrast that depends on the crystallographic orientation of each segment and so, on dislocation character. The continuous expansion of the observed loop is characteristic of pure glide motion.

A complete indexing of **R**, **S** and **T** segments of dislocations involved in fork-shaped configurations could not be entirely performed using the standard extinction method because of the fairly limited access of the *in situ* stage to various Bragg conditions (Section 2). This is why we used a combination of both a classic extinction determination of dislocation Burgers vectors and dislocation character on *postmortem* samples and a careful analysis of slip geometry and Schmid factors on *in situ* specimens.

The analysed loops are shown in Fig. 3, $t = 165$ s, and in Fig. 4, respectively, for *in situ* and *postmortem* images. In both cases, dislocation loops have highly anisotropic shapes, with contrasts strongly dependent of segment orientation, i.e. on dislocation segment character, in spite of slight shape changes due to stress relaxation in *postmortem* specimens. The characteristic shape of these loops strongly suggests that in both cases, the same type of defect is dealt with.

4. Crystallographic analysis of dislocations involved in "fork-shaped" configurations

4.1. Postmortem analysis of anisotropic loops

The analysed *postmortem* dislocation loop (labelled PM hereafter) is shown in Fig. 4.

First, the dislocation glide plane will be determined. When a glissile loop contains straight segments, the loop plane is easily determined if the orientation of any two of its segments is known. This method is applied to the PM loop, using the straight A′ and B′ segments.

A projection analysis shows that the A′ segment is perpendicular to the [1 1 0] direction, i.e. contained in the (1 1 0) plane, when the

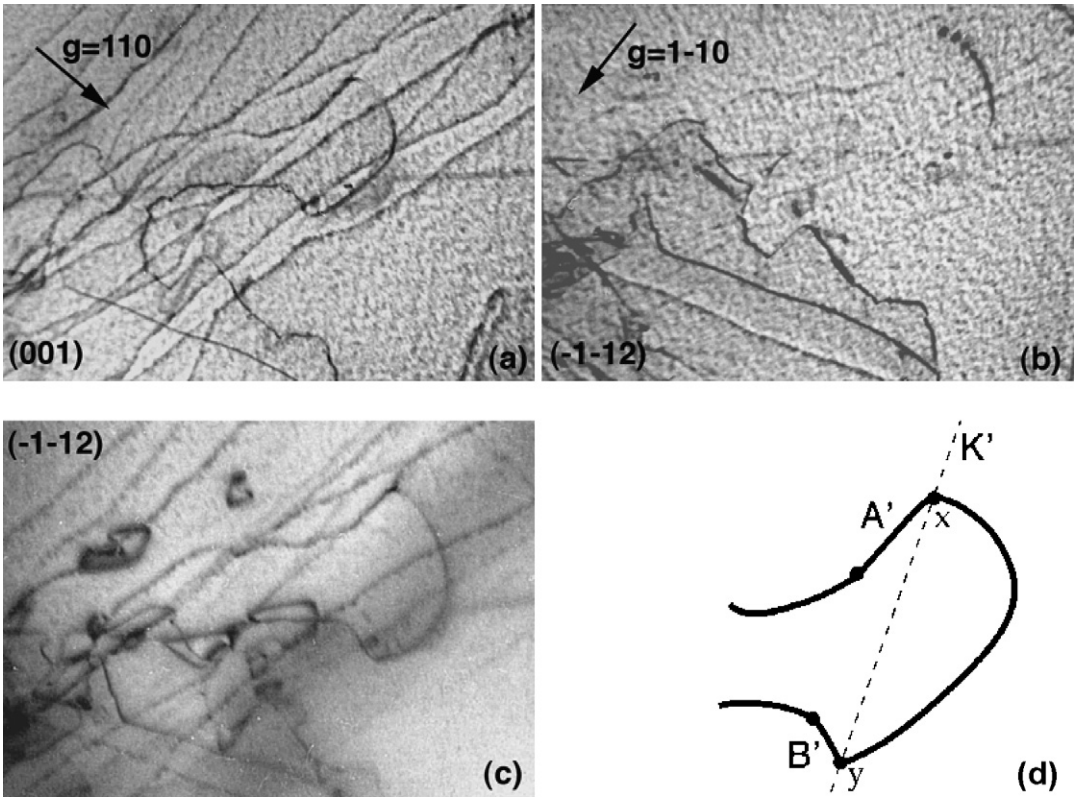

Fig. 4. An anisotropic dislocation loop. *Postmortem* study of an *in situ* deformed thin foil. (a) [1 1 −2] zone axis, multi-wave image. (b) [0 0 1] zone axis, **g** = 1 1 0. (c) [1 1 −2] zone axis, **g** = 1 −1 0: extinction conditions. A′ and B′ are straight segments (limited by points) on the dislocation loop.

image is taken close to the [0 0 1] zone axis (Fig. 4a), and is contained in the (1 1 1) plane when observed near the [1 1 −2] zone axis. As a consequence, the A′ segment is parallel to the intersection of (1 1 0) and (1 1 1) planes (Fig. 4c), i.e. parallel to [1 −1 0].

Unfortunately, this method is unsuccessful when applied to the B′ segment: for both observations near [0 0 1] and [1 1 −2] zone axes (Fig. 4c), the segment belongs to the same (1 −1 0) plane.

As no other existing segment of the loop is convenient for this purpose, an "artificial" segment is considered. In fact, the angular shape of the PM loop contains two particular points, *x* and *y* (Fig. 4d), that define a "segment" K′ belonging to the PM loop glide plane. When observed near the [0 0 1] zone axis (not shown here), the K′ segment is contained in the (1 3 0) plane. It belongs to the (1 7 4) plane in the image taken near the [1 1 −2] zone axis. The K′ segment is therefore parallel to [3 −1 1].

Finally, the PM loop glide plane, that contains both [1 −1 0] and [3 −1 1] directions, is the (1 1 −2) plane. The direction of the B′ segment can now be identified as being parallel to [1 1 1].

The Burgers vector analysis comes from two observations. First, the PM loop is in contrast with **g** = [1 1 0] (Fig. 4a) while it is invisible when **g** = [1 −1 0] (Fig. 4b). Taking into account all possible Burgers vectors for the B2 structure, only **b** = *a*[1 1 1], **b** = *a*[1 1 −1] or **b** = *a*[1 1 0] may fulfil both contrast conditions. Second, searching among these dislocations, those that may glide on the (1 1 −2) loop habit plane, gives the sought Burgers vector as being parallel to [1 1 1].

Let us recall that this kind of analysis is only valid for the determination of the Burgers vector direction, but not its absolute value; in the analysed case, it is therefore impossible to distinguish between a partial *a*/2[1 1 1] dislocation and an *a*[1 1 1] superdislocation. Yet, the continuous and easy glide of the observed dislocation loops is a major argument to consider that superdislocations are observed. Their very probable dissociation, with a partial distance of about 9 nm [19,24], is too small to be observed here due to the use of the bright field technique and the lack of sufficient camera resolution.

Finally, the PM loop has been shown as being a *b* = *a*[1 1 1] superdislocation (very probably dissociated in its glide plane) gliding in the (1 1 −2) plane. Its A′ and B′ segments have edge and screw character, respectively.

4.2. Analysis of the "fork-shaped" configuration observed in situ

The *in situ* observed anisotropic loops (Fig. 3) are "geometrically" similar to those analysed in *postmortem* conditions (Fig. 4; the "PM" loop). Even without a complete analysis of the former, the risk that they do not represent ⟨1 1 1⟩ superdislocations seems unlikely, as it was deduced from their movement (Section 3). In fact: (i) their continuous glide indicates their "perfect" character (i.e. it cannot be partial dislocations); (ii) their glide on {1 1 0} has been excluded, while that on {1 1 2} is possible (i.e. it is not a ⟨1 0 0⟩ dislocation). Therefore, in the following, it will be considered that the origin of both kinds of loops is the same. **R** and **S** segments are therefore *a*⟨1 1 1⟩ superdislocations gliding on two different {1 1 2} planes that intersect along the [−1 1 0] direction. The only {1 1 2} planes fulfilling this condition are (1 1 2) and (1 1 −2).

On the basis of the above elements, it is possible to identify the Burgers vectors of the individual dislocations involved in a "fork-shaped" configuration. Let us arbitrary decide that the **R** segment glides on (1 1 −2) (the opposite assumption should be equivalent to a symmetry with respect to the foil plane): its Burgers vector has to be $\mathbf{b_R} = \pm a[1\,1\,1]$. The **T** segment is parallel to the common direction [−1 1 0] of both the glide planes involved. Therefore, the **S** segment is an *a*⟨1 1 1⟩ dislocation gliding on the (1 1 2) plane, and its Burgers vector is $\mathbf{b_S} = \pm a[1\,1\,-1]$.

Now, it is necessary to determine the signs of **R** and **S** Burgers vectors in the coordinate system defined in Fig. 2. The Burgers vector of the **T** segment is:

$$\mathbf{b_T} = \mathbf{b_R} + \mathbf{b_S}$$

and depends on the signs of the involved $\mathbf{b_R}$ and $\mathbf{b_S}$ vectors. The deformation has been performed in tension along the [1 1 0] axis. Knowing the sense of motion for both **R** and **S** dislocations from the recorded video sequence, and using the Peach–Köehler equation, it is easy to determine the signs of all Burgers vectors. With the line directions chosen in Fig. 2, one obtains:

$$\mathbf{b_R} = a[1\,1\,1],\quad \mathbf{b_S} = a[-1\,-1\,1],\quad \text{and}\quad \mathbf{b_T} = a[0\,0\,2]$$

Thus, the **T** segment should be an edge dislocation with $\mathbf{b} = a[0\,0\,2]$ that may slip only in the (1 1 0) plane. This [0 0 2] (1 1 0) system has a zero Schmid factor in the present *in situ* experiment. This is one of the possible reasons why this segment does not move here.

Finally, let us note that this analysis is probably only correct from a "macroscopic" point of view. In fact, the interacting superdislocations are dissociated and their reactions have to be considered as a sum of two separate reactions. First, two leading partials react to give a first [0 0 1] dislocation. Then, under certain conditions, a second analogous reaction between trailing partials may take place. A more complete analysis of the possible reactions and the resulting core structures of these dislocation configurations (called "⟨0 0 1⟩ junctions") will be given in Section 5.3.

5. Discussion

5.1. On the geometry of ⟨0 0 1⟩ junctions

As shown above, the observed "fork-shaped" configurations result from a reaction between two different $a\langle 1\,1\,1\rangle$ superdislocations, gliding on different {1 1 2} planes:

$$\begin{array}{c} a[111] + a[\text{-}1\text{-}11] \rightarrow a[002] \\ \mathbf{R} \quad + \quad \mathbf{S} \quad \rightarrow \quad \mathbf{T} \end{array}$$

Somewhat similar configurations have been previously observed in deformed FeAl by other groups, always in *postmortem* studies [5,25], as summarized in Table 2. Munroe and Baker [25] have studied different binary, boron-free Fe–Al alloys, with Al content between 34 and 45 at.%. Their *postmortem* observations of dislocation configurations after room temperature compression show interactions of ⟨1 1 1⟩ dislocations, gliding on {1 1 0} planes, reacting into an $a\langle 0\,0\,2\rangle$ dislocation, that may dissociate by glide into a pair of identical ordinary edge ⟨0 0 1⟩ dislocations. The $a\langle 0\,0\,2\rangle$ dislocation is aligned along another ⟨0 0 1⟩ direction that belongs to the same {1 0 0} plane, and so, characterised by a {1 0 0} glide plane, as shown on Fig. 5a.

Table 3
Schmid factor F_s values for different possible slip systems. Glide on {1 1 0} or {1 1 2} planes is considered. Tensile axis parallel to the [1 1 0] direction.

Dislocation	Burgers vector	Slip plane	F_s
R	[−1 −1 −1]	(1 −1 0)	0
R	[−1 −1 −1]	(1 0 −1)	−0.41
R	[−1 −1 −1]	(0 1 −1)	−0.41
R	[−1 −1 −1]	(1 −2 1)	0.24
R	[−1 −1 −1]	(−2 1 1)	0.24
R	[**−1 −1 −1**]	(**1 1 −2**)	**−0.47**
S	[−1 −1 1]	(1 −1 0)	0
S	[−1 −1 1]	(0 1 1)	−0.41
S	[−1 −1 1]	(1 0 1)	−0.41
S	[**−1 −1 1**]	(**1 1 2**)	**−0.47**
S	[−1 −1 1]	(−1 2 1)	−0.24
S	[−1 −1 1]	(2 −1 1)	−0.24

The bold values correspond to the highest values of Schmid factor.

The observations by Morris and Morris [5], also performed in a binary, B-free Fe–40Al alloy, but deformed at 500 °C, are in good agreement with [25]. Still, the determination of the glide planes of reacting ⟨1 1 1⟩ dislocations remains uncertain. Finally, using crystallographic considerations, the authors conclude that {1 1 0} glide planes are more probable than {1 1 2} ones, which should lead to the same configuration as observed by Munroe and Baker [25].

Our present observations unambiguously lead to a somewhat different reaction, resulting from the fact that ⟨1 1 1⟩ superdislocations glide in the present case on {1 1 2} planes and not on {1 1 0} ones. As a consequence, the line direction of the resulting $a\langle 2\,0\,0\rangle$ dislocation is of ⟨1 1 0⟩ type (Fig. 5b).

This difference may come from at least one of the several possible reasons, namely: (i) the orientation of the tensile axis in the present work may favour {1 1 2} slip systems, (ii) the present observation was performed at a higher temperature, and (iii) the studied alloy was doped with boron and alloyed with nickel. The possible effects of all these factors are discussed below.

5.2. {1 1 0} or {1 1 2} nature of superdislocation slip planes

It is commonly agreed that superdislocation glide in B2–FeAl mostly occurs on {1 1 0} planes, while {1 1 2} glide remains anecdotic, at least at low temperatures. However, specific orientations of the tensile axis may modify the active slip systems. In our case, superdislocation glide on {1 1 2} slip planes is consistent with Schmid factors computed for all possible slip systems (Table 3). Yet, the highest Schmid factor values obtained for {1 1 2} planes are only

Table 2
Different observations of ⟨1 1 1⟩ reactions in B2-ordered FeAl.

composition of studied alloys (%at. Al)	ref.	deformation temperature	glide planes of reacting a<111>	resulting dislocation: Burgers vector	resulting dislocation: Line vector	glide plane of the resulting dislocation
34 40 45	[25]	25°C	{110}	<001> edge	<001>	{100}
40	[5]	500°C	{110} or {112} ?	<001> edge		{100}
40 + 100 ppm B + 4 % at. Ni	this work	600°C	{112}	<001> edge	<110>	{110}

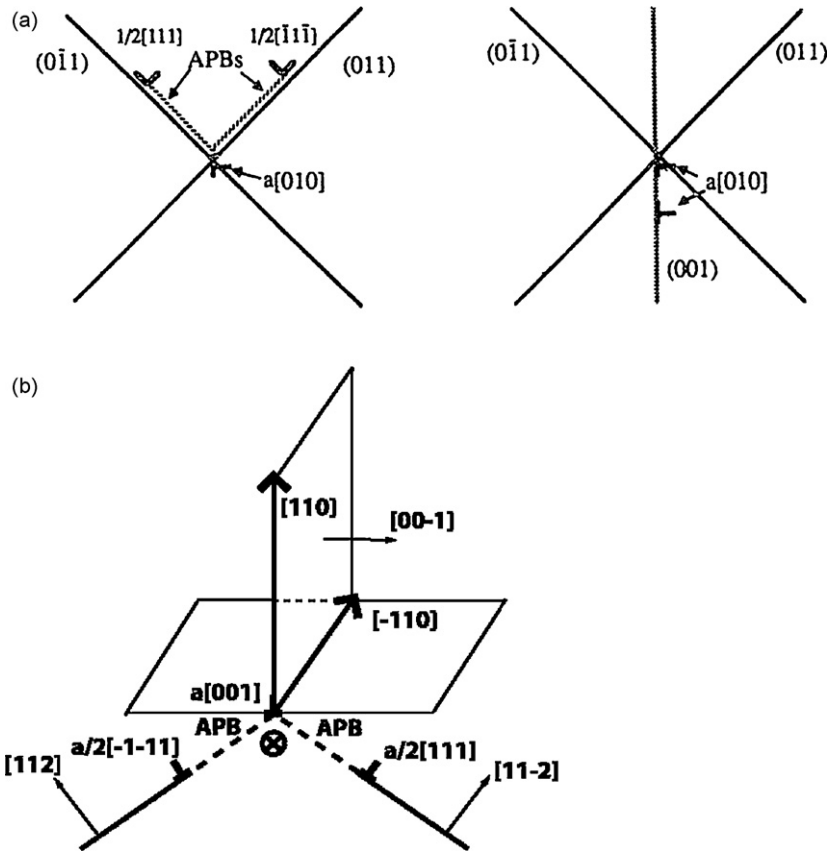

Fig. 5. Schematic illustration of the formation of $a\langle 0\,0\,2\rangle$ dislocations. (a) Munroe and Baker work [25]; (b) present work.

slightly larger than that for a set of {1 1 0} planes, and {1 1 0} glide cannot be excluded on the basis of Schmid factors alone.

It seems reasonable to consider that the activation of {1 1 2} slip in the present case may also be due to both test temperature and intrinsic properties of the studied material, and not just to sample orientation. Especially, {1 1 2} glide of superdislocations in FeAl is favoured at high temperatures [5]. A recent work [26] seems to indicate that at room temperature, boron addition promotes {1 1 2} glide of superdislocations. Our observation of {1 1 2} glide is in agreement with these two results, and is therefore probably still valid for other crystal orientations and for polycrystalline alloys. Finally, nickel addition increases the APB energy and consequently, decreases the dissociation distance between $a/2\langle 1\,1\,1\rangle$ superpartials [10,15]. In agreement with the estimates by Munroe and Baker [25], the formation of $\langle 1\,0\,0\rangle$ junctions is energetically more favourable for lower superpartials distances, nickel in FeAl should really promote this kind of dislocation reactions.

5.3. Core structure of $\langle 0\,0\,1\rangle$ junctions

The formation of an $a\langle 0\,0\,2\rangle$ dislocation as described in Section 5.1 is only a "macroscopic" approach of the possible reaction. Yet, it seems unlikely in terms of line energy. Considering the dissociation of superdislocations into superpartials allows a more detailed and acceptable analysis of their reactions. We are sure that a reaction between both leading partials takes place, giving an $a\langle 0\,0\,1\rangle$ ordinary dislocation at the apex of intersecting slip planes (Fig. 5b), according to:

$$\frac{a}{2}[1\,1\,1]+\frac{a}{2}[-1\,-1\,1]=a[0\,0\,1] \qquad \text{(a)}$$

The mobility of the resulting dislocation is low, as it can only leave the intersection of slip planes by a (1 1 0) glide (improbable when considering its repulsive interactions with trailing $a/2\langle 1\,1\,1\rangle$ superpartials), or climb. However, a new reaction between both trailing partials, analogous to (a), seems improbable, since the interaction between the newly formed $a[0\,0\,1]$ dislocation and the trailing $a/2\langle 1\,1\,1\rangle$ superpartials is repulsive. Finally, the structure of the complete [0 0 2] junction is likely to consist of an inversed-V-shaped non-planar core, with the $a[0\,0\,1]$ dislocation sitting at the apex, and separated from the two trailing $a\langle 1\,1\,1\rangle$ partials by APB ribbons (Fig. 5b). This configuration is somewhat similar to the well-known Lomer–Cottrell barrier in the FCC structure [27], where stacking fault ribbons are replaced by APB ones. This configuration is therefore probably sessile.

Such a scenario may be another reason why **T** does not move in Fig. 3, $t = 81$ s to $t = 110$ s.

5.4. Possible role of $\langle 0\,0\,1\rangle$ junctions on mechanical properties of FeAl

It is obvious that the mobility of $\langle 0\,0\,1\rangle$ junctions with an inversed-V-shaped non-planar core structure is low. Now, let us consider the different possibilities of modification of this complex core structure.

The first $a[0\,0\,1]$ dislocation, formed by a reaction of both leading superpartials, can only glide in the (1 1 0) plane. Its motion is difficult due to the repulsive interactions with the trailing superpartials; moreover, this kind of movement, if it exists, should be observed in the experiment as a lateral movement of the **T** segment. No similar movement was observed in this study; the only "movement" of the **T** segment that was observed is accompanied by the slow vanishing of its contrast, suggesting a motion towards the surface, probably due to image forces.

If the glide is prevented, the only opportunity to obtain a dislocation motion is *via* its climb. For the studied $a[0\,0\,1]$ dislocation, it would make it leave its glide plane, and follow the [1 1 0] direction. In these conditions, the reaction of both trailing superpartials becomes possible: finally, a "pile-up" of two similar $a[0\,0\,1]$ edge dislocations, gliding in parallel (1 1 0) planes, is formed. This is a classic, stable configuration of edge dislocations. At a larger scale, it is analogous to the Burgers model of low angle grain boundary. Under an external stress such a configuration of edge dislocations is mobile, gliding in parallel slip planes. The situation is more complicated in the studied case: both [0 0 1] dislocations are not free; they belong to a complex configuration containing two reacting $a\langle 1\,1\,1\rangle$ superdislocations. That is why the whole configuration of the $\langle 0\,0\,1\rangle$ junction remains sessile. Yet, if both reacted $\langle 1\,0\,0\rangle$ segments are long enough, their independent glide in their glide planes becomes probable.

Now, the effects of temperature on the structure and behaviour of $\langle 0\,0\,1\rangle$ junctions have to be contemplated. At low or intermediate temperatures, sessile, straight $a\langle 0\,0\,1\rangle$ dislocations lying in slip planes of superdislocations may be responsible for pile-up induced stress concentrations and for possible brittle cleavage, as suggested by Munroe and Baker [25].

At higher temperatures, the climb effect can become significant, especially in FeAl, in which high concentrations of thermal vacancies may be easily attained. Therefore, it may be reasonably expected that $\langle 0\,0\,2\rangle$ dislocations become mobile. Thermal activation may indeed allow local recombination of the core, that may then extend sideways under stress, as kink pairs do on screw dislocations in bcc metals for instance. However, in contrast with the bcc case, the recombined segment would be unstable and thus immediately decompose into two identical (and hence repulsive) ordinary $\langle 0\,0\,1\rangle$ dislocations without any APB between them, that would be free of gliding in their common $\{1\,1\,0\}$ slip plane.

Let us note that intersections at high temperatures of pre-existing $\langle 1\,1\,1\rangle$ superdislocations would allow a large scale production of $\langle 0\,0\,1\rangle$ ordinary dislocations. This last suggestion may account for the change in slip direction above the YSA peak temperature.

6. Conclusions

1. "Fork-shaped" dislocation configurations, observed during *in situ* straining TEM experiments at 600 °C in an FeAl alloy containing boron and nickel result from a reaction of two different $a\langle 1\,1\,1\rangle$ superdislocations gliding on crossing $\{1\,1\,2\}$ planes. This reaction leads to a $\langle 0\,0\,1\rangle$ junction, formed by a pair of a $\langle 0\,0\,1\rangle$ dislocations (Fig. 2), following a scheme of type:

$$a[1\,1\,1] + a[-1\,-1\,1] \rightarrow a[0\,0\,2]$$

2. Some similar configurations have been previously observed [5,16] in binary FeAl in *postmortem* analyses. However, important differences have been found in the crystallographic characteristics of involved dislocations. In particular, in this work, the reacting dislocations have been shown to glide on $\{1\,1\,2\}$ planes, which are less common than the standard $\{1\,1\,0\}$ ones, previously observed. Both the specific thin foil orientation and experimental conditions (presence of boron in the studied alloy and/or the high testing temperature) may explain this effect.
3. Even if all individual dislocations involved are glissile, the complex geometry of the $\langle 0\,0\,1\rangle$ junction gives it a sessile character. Thus, this kind of junction may play a locking role for dislocation movement in FeAl. In particular, following a previous idea by Munroe and Baker [25], the presence of these kinds of junctions may be involved in the room temperature cleavage brittle fracture of FeAl. Their possible role for the yield strength anomaly still remains to be defined.

Acknowledgements

The authors are grateful to Beatrice Doisneau-Cottignies, LTPCM/INPG Grenoble, for performing the *in situ* TEM experiments and for all the help she gave us during this work.

The authors kindly acknowledge the financial support of this work by the Region Rhône-Alpes "*Thematiques prioritaires*" program, under the contract No. 00 81 51 41.

Appendix A. Supplementary data

Supplementary data associated with this article can be found, in the online version, at doi:10.1016/j.jallcom.2010.03.058.

References

[1] I. Baker, P.R. Munroe, Int. Mater. Rev. 42 (1997) 181.
[2] D.G. Morris, C.T. Liu, E.P. George, Intermetallics 7 (1999) 1059.
[3] F. Louchet, Philos. Mag. A 72 (1995) 905.
[4] E.P. George, I. Baker, Intermetallics 6 (1998) 759.
[5] D.G. Morris, M.A. Morris, Intermetallics 5 (1997) 245.
[6] K. Yoshimi, S. Hanada, M.H. Yoo, Acta Mater. 43 (1995) 4141.
[7] O. Calonne, A. Fraczkiewicz, F. Louchet, Scripta Mater. 43 (2000) 69.
[8] M. Kupka, J. Alloys Compd. 437 (2007) 373.
[9] U. Messerschmidt, M. Bartsch, Ch. Dietzsch, Intermetallics 14 (2006) 607.
[10] R.C. Crawford, Philos. Mag. A 33 (1976) 529.
[11] T. Yamagata, H. Yoshida, Mater. Sci. Eng. 12 (1973) 95.
[12] M.A. Crimp, K. Vedula, Philos. Mag. A 63 (1991) 559.
[13] K. Yoshimi, S. Hanada, M.H. Yoo, Intermetallics 4 (1996) S159.
[14] J. Baker, J.A. Horton, Philos. Mag. A 67 (1993) 479.
[15] M.H. Yoo, K. Yoshimi, S. Hanada, Acta Mater. 47 (1999) 3579.
[16] Y. Umakoshi, M. Yamaguchi, Philos. Mag. A 41 (1980) 573.
[17] Y. Yang, I. Baker, Intermetallics 6 (1998) 167.
[18] C.L. Fu, Y.Y. Ye, M.H. Yoo, Phys. Rev. B 48 (1993) 6712.
[19] D. Colas, A. Fraczkiewicz, F. Louchet, Intermetallics 15 (2007) 85.
[20] F. Louchet, B. Doisneau-Cottignies, O. Calonne, A. Fraczkiewicz, M. Janecek, N. Guelton, JOM 203 (2001) 84.
[21] B.A. Bilby, R. Bullough, E. Smith, Proc. Roy. Soc. A231 (1955) 263.
[22] A. Howie, N.J. Whelan, Proc. Roy. Soc. A267 (1962) 206.
[23] Video sequence from the in situ experiment.
[24] M.F. Savage, R. Srinivasan, M.S. Daw, T. Lograsso, M.J. Mills, Mater. Sci. Eng. A258 (1998) 20.
[25] P.R. Munroe, I. Baker, Acta Mater. 39 (1991) 1011.
[26] T. Cordonnier, A. Fraczkiewicz, private communication.
[27] J.P. Hirth, J. Lothe, Theory of Dislocations, Wiley, New York, 1982, p. 799.